Time-reversible dissipative attractors in three and four phase-space dimensions

H. A. Posch
Institute for Experimental Physics, University of Vienna, Boltzmanngasse 5, Wien A-1090, Austria

Wm. G. Hoover
Department of Applied Science, University of California at Davis/Livermore, Livermore, California 94551-7808
and Lawrence Livermore National Laboratory, Livermore, California 94551-7808

(Received 14 February 1997)

We establish the dissipative nature of several three- and four-dimensional time-reversible phase-space flows and study their ergodicity. Three- and four-dimensional generalizations of the equilibrium Nosé-Hoover oscillator provide the simplest robust continuous models for time-reversible nonequilibrium dissipative systems. Most such systems exhibit discontinuities or periodicities. We have discovered one set of four ordinary differential equations which is simultaneously robust, time-reversible, dissipative, and ergodic, with solutions free of any discontinuities and periodicities. [S1063-651X(97)15206-0]

PACS number(s): 05.45.+b, 02.70.−c, 05.70.Ln, 47.27.Te

I. INTRODUCTION

Time-reversible computer algorithms, designed to simulate nonequilibrium dissipative molecular dynamics, began to be developed about 25 years ago [1,2]. The Newtonian atomistic and boundary forces were supplemented with constraint and driving forces, so as to simulate diffusive, deformational, and heat-conducting flows. Though in many cases the resulting nonequilibrium algorithms were time-reversible, this property was not, at first, stressed. The nonequilibrium simulations evolved in parallel with rapid developments in nonlinear dynamics and deterministic chaos [3], but only rarely were connections made, and parallels drawn, linking these fields together [4].

Theoretical analyses of nonequilibrium flows are complicated by the fractal nature of the corresponding phase-space distributions. The apparent paradox that time-reversible motion equations can provide dissipative irreversible phase-space flows motivated the study of simple few-body systems, driven from equilibrium but thermally constrained, so as to generate stationary nonequilibrium states. About ten years ago these studies revealed the way in which time-reversible equations of motion can lead to dissipative phase-space flows [5]. Such flows typically connect a Lyapunov-unstable multifractal repellor source to a geometrically similar strange attractor sink. The repellor and attractor are time-reversed images of each other.

The first problem studied, the field-driven regular ''Galton board'' or ''Lorentz gas,'' corresponds to the motion of a particle through a regular lattice of scatterers [6–8]. The phase space describing the collisions of the moving particle with the scatterers is divided into several contiguous regions. Each of these regions represents those trajectories which link a particular pair of nearby scatterers—these can be first, second, or third neighbors of each other—in a regular two-dimensional triangular lattice. For low to moderate field strengths, the phase-space distribution is ''ergodic'' [6–8], covering the full energy surface, but with a fractal probability density which is everywhere singular. Not only the collisional surfaces which separate the various scattering regions, but also the periodic boundaries associated with the lattice, are sources of complexity in analyzing the Galton board [6,8].

The one-dimensional ''Galton staircase'' problem is less singular [9]. It describes a thermostatted pendulum, driven by a torsional external field E and under the influence of gravity. The strength of the gravitational field is proportional to the parameter ε:

$$\dot{q}=p/m; \quad \dot{p}=E-\varepsilon\sin q-\zeta p; \quad \dot{\zeta}=[(p^2/mkT)-1]/\tau^2.$$

The thermostat variable, ζ, plays the rôle of a control variable. This control variable implements the thermal constraint $\langle p^2\rangle = mkT$, where k is Boltzmann's constant and T is the temperature. τ is a free parameter, the thermostat relaxation time. Periodic boundaries are used for the pendulum location q, with $-\pi<q<+\pi$. A typical chaotic trajectory repeatedly leaves and reenters the periodic phase-space cell. Note the time reversibility of these equations. At any time a trajectory going forward in time can be made to trace out its past history, by reversing the signs of p and ζ.

For simplicity, it is desirable to avoid subdividing phase space into separate regions, such as those representing the different types of collisions which can occur in the Lorentz gas. It is equally desirable to avoid the geometric complexity associated with the periodic boundary conditions common to both the examples just discussed. Such divisions and periodicities complicate theoretical analyses [8,10]. A relatively simple problem, which lacks both these complicating features, is the two-temperature motion of a particle confined by a two-dimensional angle-dependent potential [11]. Unfortunately, that motion occurs in a six-dimensional phase space, $\{x,y,p_x,p_y,\zeta_x,\zeta_y\}$, making visualization out of the question.

We know of only one example in the literature of a three-dimensional continuous flow which is not only time reversible and dissipative but also free of singularities and periodicities. It was discovered by Sprott, though its time reversibility was passed over, unnoticed [12]. The simplest of all the chaotic flows studied by Sprott, albeit nondissipative, turned out to be the familiar equilibrium Nosé-Hoover

oscillator [13]. Of the remaining 18 topological types of chaotic flows, only a single one, Sprott's case D, is simultaneously time reversible and dissipative:

$$\dot{x} = -y; \quad \dot{y} = x + z; \quad \dot{z} = xz + 3y^2.$$

To reverse this flow x and z must be odd functions of time, while y must be even. However, the flow is not particularly robust and has a tendency to diverge if the initial conditions are chosen far from the origin. For initial conditions close to the origin and with all possible sign combinations $\{x,y,z\} = \{\pm 0.1, \pm 0.1, \pm 0.1\}$, one finds that the combination $\{---\}$ provides a stable limit cycle, with a period just less than 20; the combination $\{+--\}$ diverges; the other six sign combinations do lead to a fractal attractor with an information dimension $D_I = 2.078$. This dimension is much less than the embedding dimension D of the space, 3. The relatively large difference, 0.922, reflects the relative rarity of convergent solutions of Sprott's equations, and is not at all typical of thermostatted physical systems. Physical systems, for conditions close to equilibrium at least, typically have attractor dimensions close to the embedding dimension of their equilibrium phase space. In view of this delicate convergence, Sprott's equations are not a promising model for physical dissipative systems.

The stimulation provided by a recent workshop and conference on time reversibility [14] led us to study three distinct classes of similar dynamical systems which are free from such complicating singularities, divergence problems, and periodicities. Each of these systems simultaneously exhibits time reversibility and dissipation. We adopt the usual meaning of time reversibility: for any trajectory proceeding in the positive time direction there exists a reversed trajectory, obeying exactly the same motion equations, but with different initial conditions. We call a system ''dissipative'' if, from a continuous distribution of initial conditions, a phase-space strange attractor is generated.

In the following three sections we consider a series of nonequilibrium systems based on the robust and well-characterized equilibrium Nosé-Hoover oscillator [13]. We originally selected this model as the simplest prototypical example of Nosé's approach to thermostatted dynamics [15]. The model is also the field-free small-amplitude limit of the Galton staircase model mentioned before. The equilibrium Nosé-Hoover oscillator is described by a three-dimensional phase-space flow, with the coordinate q and momentum p controlled by a time-reversible friction coefficient ζ:

$$\dot{q} = p/m; \quad \dot{p} = -\kappa q - \zeta p; \quad \dot{\zeta} = [(p^2/mkT) - 1]/\tau^2.$$

In these equations m is the particle mass, κ is the force constant, and kT is, as before, the product of Boltzmann's constant and the temperature. It is noteworthy that these equations of motion preserve a generalized form of Gibbs' equilibrium canonical phase-space distribution. However, individual oscillator trajectories cannot access the complete distribution because the flow is not ergodic. The phase-space distribution is instead partitioned by the flow equations into a single chaotic ''sea,'' which is threaded through by a countable infinity of regular quasiperiodic regions. Each of these regular regions surrounds a stable periodic orbit in the (q,p,ζ) space. The Nosé-Hoover oscillator has a Hamiltonian basis [15], and its time-averaged motion conserves occupied phase volume, rather than shrinking onto an attractor. It is not dissipative, and the time-averaged friction coefficient ζ, describing the comoving rate of phase volume shrinkage, vanishes: $\langle \zeta \rangle = 0$.

TABLE I. Characteristics of three time-reversible dissipative generalizations of the three-dimensional equilibrium Nosé-Hoover oscillator model. The embedding dimensions D are given. The presence or absence of smooth weight functions w, finite thermal smoothing lengths h, control of the kinetic energy and its square, and ergodicity, are all indicated by a + or −.

Case	D	w	h	$\langle p^2 \rangle$	$\langle p^4 \rangle$	Ergodic
I	4	+	−	+	−	−
II	3	−	+	+	−	−
III	4	−	+	+	+	+

All three nonequilibrium generalizations of the Nosé-Hoover oscillator, which we study in the following, produce strange attractors in three-or-four-dimensional phase spaces. The first uses two spatially localized thermostats, described by compact weighting functions $\{w_T(q)\}$. The other two generalizations correspond to models which interpolate between two different temperatures with a switching function of range h. The last of the models, perhaps the most promising from the standpoint of analysis, uses control of both the temperature and its fluctuation. The differing properties of the three cases are summarized in Table I.

II. NOSÉ-HOOVER OSCILLATOR WITH SPATIALLY WEIGHTED THERMOSTATS

Though many-body generalizations of the Nosé-Hoover approach have been applied to a variety of nonequilibrium flows, the simplest example so far considered involved a six-dimensional phase space [11]. By using two separate thermostatted regions, in one space dimension, it is possible to reduce the phase-space dimensionality to four. This generalization of the Nosé-Hoover oscillator to a two-temperature dissipative nonequilibrium model requires two separate control variables, ζ_C and ζ_H. Two separate weighting functions, w_C and w_H, describe the spatial and temporal extents of the thermostatted regions [1]. In the time-independent case, considered here, the weighting functions depend only upon the oscillator coordinate q. A convenient choice for the $\{w_T(q)\}$, with continuous first and second derivatives, is Lucy's [16] smooth-particle weighting function

$$w_T = (1 - r_T)^3(1 + 3r_T) \quad \text{for } 0 < r_T < 1; \quad r_C = |q+1|; \quad r_H = |q-1|,$$

with $T \in \{C,H\}$. The temperatures within the cold and hot regions, centered at $q = -1$ and $q = +1$, respectively, are imposed by ζ_C and ζ_H, which act with characteristic relaxation times τ_C and τ_H. With the simplest choice for the relaxation times, $\tau_C = \tau_H = \tau$, the equations of motion for the two-temperature oscillator system are as follows:

$$\dot{q}=p/m; \quad \dot{p}=-\kappa q-(w_C\zeta_C+w_H\zeta_H)p;$$

$$\dot{\zeta}_C=w_C[(p^2/mkT_C)-1]/\tau^2;$$

$$\dot{\zeta}_H=w_H[(p^2/mkT_H)-1]/\tau^2.$$

Though we have not carried out a comprehensive study of this four-dimensional flow, we have confirmed that it typically generates a time-reversible dissipative strange attractor over a wide range of conditions. These atttractors are even more complex than their equilibrium relatives. Within the attractors are many embedded regions which, in turn, support a wide variety of quasiperiodic orbits. This topological complexity, in a four-dimensional space, argues against using the spatially weighted thermostatted oscillator as a paradigm for many-body stationary nonequilibrium states.

III. NOSÉ-HOOVER OSCILLATOR WITH CONTINUOUSLY VARIABLE TEMPERATURE

An even simpler nonequilibrium thermostatted oscillator results if temperature is taken to be a smooth function of the coordinate,

$$T=T(q)=T_0[1+\varepsilon\tanh(q/h)].$$

This nonequilibrium system requires only three phase-space dimensions if, just as in the equilibrium case, temperature is controlled by a single friction coefficient:

$$\dot{q}=p/m; \quad \dot{p}=-\kappa q-\zeta p; \quad \dot{\zeta}=[p^2-mkT(q)]/(mkT_0\tau^2).$$

We choose the hyperbolic tangent so as to switch the reduced temperature smoothly from $1-\varepsilon$, for $(q/h)\ll 0$, to $1+\varepsilon$, for $(q/h)\gg 0$. The temperature difference, $T_{+\infty}-T_{-\infty}\equiv 2\varepsilon T_0$, the spatial width of the thermal transition region h, and the relaxation time τ are all fixed parameters describing the system.

It is interesting to note that applying the concept of a space-dependent temperature to Nosé's original Hamiltonian, or to Dettmann's recent modification of it, in the extended phase space, $\{Q,P,s,P_s\}$, leads to equations of motion slightly different from those used here. The difference is described in more detail in the Appendix. We choose the equations of this section for our studies, because they are an obvious and simple generalization of the equilibrium case, with all the generic properties shown by dissipative many-body systems: Lyapunov instability, dissipative shrinking of comoving phase volume, and multifractal phase-space density.

The equilibrium state for the thermostatted oscillator corresponds to the special case $\varepsilon=0$. The corresponding dynamics, though relatively complex, is only three-dimensional, and so has been exhaustively explored [13]. The equilibrium phase space is partitioned into two different sorts of regions: (i) a countable infinity of periodic tubular regions, centered on regular orbits and (ii) a single unstable chaotic region in which all the tubes are embedded. The measures of the two sorts of regions—that is, the total phase volumes, weighted with Gibbs' canonical weight, $e^{-H/kT}$—are comparable.

In the nonequilibrium case, it is desirable to reduce this complexity, as much as is possible, by studying the region in which the chaotic instability typical of many-body systems is maximized. Figure 13 of Ref. [13a] indicates that a maximum value for the largest Lyapunov exponent, λ_1, corresponds to a relaxation time, τ, of about 0.5. We accordingly choose $\tau=0.5$ for our numerical studies. To optimize the accuracy of our trajectory calculations we use a fourth-order Runge-Kutta integrator, with reduced time steps of order 0.005. The expected single-step error for such a time step, $0.005^5/5!=3\times 10^{-14}$, is about equal to the truncation errors inherent in double-precision floating point arithmetic. For a few parameter sets we experimented also with quadruple-precision, thirty-digit accuracy, and time steps as small as 0.0001. Since we always found the same asymptotic behavior—a chaotic sea or a limit cycle—as with double precision arithmetic, we do not distinguish between these methods in the following.

The results given in Table II indicate that a gradual transition between the hot and cold oscillator regions tends to promote chaos, with a very small or very large temperature difference more likely to generate regular quasiperiodic solutions. Very long runs establish that trajectories with a range $h=2$ and a reduced temperature difference $2\varepsilon=0.4$ are likely to be asymptotically regular, rather than chaotic, though they may exhibit a chaotic transient lasting for many millions of time steps. This is demonstrated in Fig. 1 by the Poincaré map at the plane $x=0$, for the parameters $h=2$, $\tau=0.5$, and $\varepsilon=0.2$, with initial conditions $\{q,p,\zeta\}=\{0,3.015,0\}$. For the first 380 000 time units (76 million time steps) the oscillating particle seems to fill the chaotic sea randomly, only to settle, finally, on a 20-point periodic orbit in the Poincaré plane (indicated by diamonds in Fig. 1). These 20 repeating points are stable, to machine accuracy, with respect to small perturbations. Obviously the whole chaotic sea acts as a ''basin of attraction'' for these periodic orbits, with a vanishing maximum Lyapunov exponent in flow direction, and two weakly negative exponents transverse to the flow. Even quadruple-precision arithmetic asymptotically leads to the same results.

In the simpler, and perhaps more generally interesting stationary chaotic cases, the Lyapunov exponents are close to the corresponding equilibrium values, even in the case that the temperature varies by a factor of 9. The rate of energy dissipation is determined by the time-averaged thermostat variable,

$$\langle\zeta\rangle=-(\lambda_1+\lambda_2+\lambda_3),$$

equal to the negative sum of all Lyapunov exponents. Though symmetry would suggest dissipation varying as the square of the temperature difference, for ε not too large, there is really no evidence for such a behavior in the range of ε treated in Table II. In most cases, the convergence of the Lyapunov exponents is slow. Two examples for Poincaré maps on the plane $\zeta=0$ are shown in Figs. 2 and 3. One peculiarity of these maps is a pair of slightly-curved gaps with vanishing phase-space flux across the Poincaré plane near $p=\pm 1$. Points on these curves would be characterized by $\dot{\zeta}=0$. All Poincaré points, for which $\dot{\zeta}<0$, are located between these two curves. All points with $\dot{\zeta}>0$ lie outside

TABLE II. Dependence of the Lyapunov spectrum $\{\lambda_1,\lambda_2,\lambda_3\}$ and the time-averaged dissipation $\langle\zeta\rangle$ on the range h and strength ε of the temperature difference for the harmonic oscillator with space-dependent thermostat of Sec. III. The results tabulated here correspond to simulations carried out for a time of at least 10 million time units, using a time step 0.005. The characteristic time τ associated with the temperature control variable is 0.50 in every case. The initial condition was chosen as $(q,p,\zeta)=(0,4,0)$. The information dimension D_I is determined according to Kaplan and Yorke's conjecture. All numbers are given in the reduced units introduced in Sec. III. The standard deviation for the nonvanishing exponents is typically ± 0.0005 for a chaotic trajectory, and less than ± 0.0001 for a limit-cycle solution. We applied Benettin's method to obtain all three time-averaged Lyapunov exponents, as is described in Refs. [21–23].

h	ε	λ_1	λ_2	λ_3	$\langle\zeta\rangle$	D_I
2.00	0.2	0	−0.0022	−0.0021	0.0042	1
2.00	0.4	0.0458	0	−0.0621	0.0163	2.737
2.00	0.6	0.0401	0	−0.0787	0.0387	2.509
2.00	0.8	0	−0.0016	−0.0015	0.0031	1
1.80	0.2	0	−0.0017	−0.0017	0.0035	1
1.50	0.2	0.0419	0	−0.0476	0.0057	2.880
1.00	0.2	0.0485	0	−0.0597	0.0112	2.812
1.00	0.4	0.0508	0	−0.0725	0.0217	2.701
1.00	0.6	0.0410	0	−0.0730	0.0320	2.561
1.00	0.8	0	−0.0066	−0.3574	0.3641	1
0.50	0.2	0.0508	0	−0.0645	0.0136	2.789
0.50	0.4	0.0176	0	−0.0319	0.0144	2.550
0.50	0.6	0	−0.0903	−0.0974	0.1877	1
0.50	0.8	0	−0.1843	−0.2470	0.4313	1
0.25	0.2	0	−0.0254	−0.0255	0.0509	1
0.25	0.4	0	−0.0296	−0.0296	0.0592	1
0.25	0.6	0.0397	0	−0.0473	0.0076	2.840
0.25	0.8	0	−0.0172	−0.0172	0.0344	1

them. The existence of a vanishing density of points on such curves does *not* imply a vanishing phase-space density there. It is only an indication of a vanishing phase-space flux, the product of the density with the phase-space velocity, perpendicular to the Poincaré plane. The appearance of these lines can be avoided altogether by plotting directly the phase-space density in a narrow section of phase space symmetrically placed around the Poincaré plane. This will be discussed in the following section.

We conclude that, although simpler and of lower phase-space dimension than the oscillator with spatially weighted thermostats in Sec. II, the nonequilibrium oscillator with a continuously varying temperature still suffers from excessive

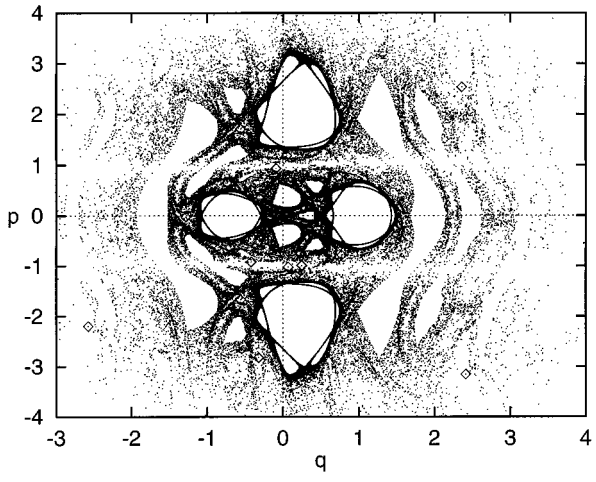

FIG. 1. Poincaré map for the thermostatted oscillator of Sec. III, where $T(q)=1+0.2\tanh(q/2)$, and where the thermostat relaxation time τ has been set equal to 0.5. The Poincaré plane is defined by $\zeta=0$. 120 000 points of the transient trajectory are shown. The 20 points of the asymptotic limit cycle are indicated by diamonds. All numbers are given in the reduced units of Sec. III.

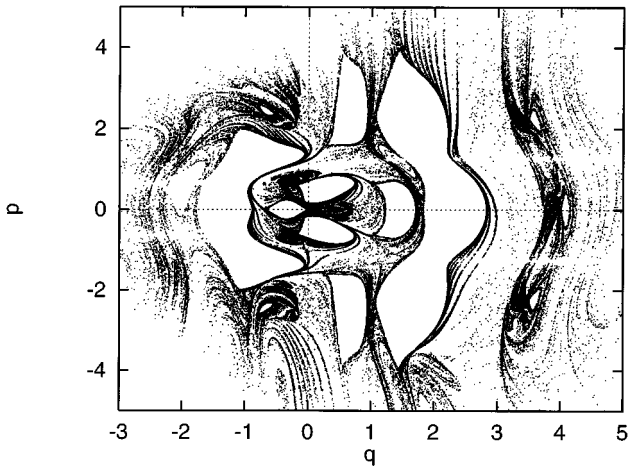

FIG. 2. Poincaré map for a chaotic solution of the thermostatted oscillator of Sec. III, with $T(q)=1+0.6\tanh(q/1)$, with the thermostat relaxation time τ set equal to 0.5, and with initial conditions $\{q,p,\zeta\}=\{0,4,0\}$. All numbers are given in the reduced units of Sec. III.

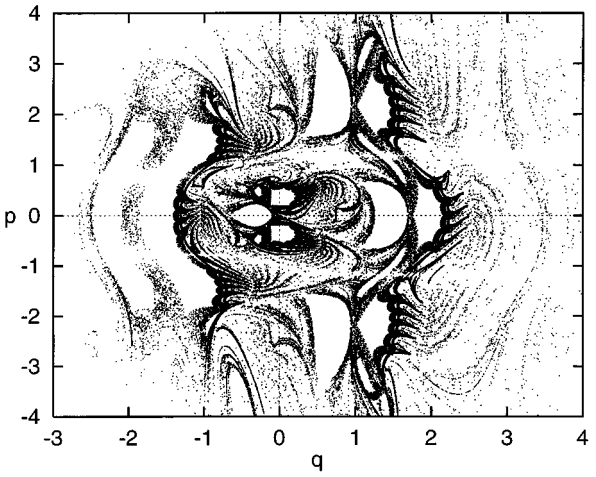

FIG. 3. Poincaré map for a chaotic solution of the thermostatted oscillator of Sec. III, with $T(q)=1+0.4\tanh(q/0.5)$, with the thermostat relaxation time τ set equal to 0.5, and with initial conditions $\{q,p,\zeta\}=\{0,4,0\}$. All numbers are given in the reduced units of Sec. III.

topological complexity, as the examples in the figures, just discussed, establish.

IV. NOSÉ-HOOVER OSCILLATOR WITH SIMULTANEOUS CONTROL OF K AND K^2

A way to avoid the phase-space complexity of all the foregoing models was discovered quite recently [17]. Consider controlling both the kinetic energy, $K=p^2/2m$, and its square, by using two independent control variables. This is equivalent to controlling both the second and the fourth moments of the momentum p. Then, an interesting four-dimensional flow results for the harmonic oscillator subjected to the same hyperbolic-tangent temperature-switching function as in the last section:

$$\dot{q}=p/m; \quad \dot{p}=-\kappa q-\zeta p-\xi p^3/(mkT_0);$$

$$\dot{\zeta}=[p^2-mkT(q)]/(mkT_0\tau^2);$$

$$\dot{\xi}=(p^4-3mkT_0p^2)/(mkT_0\tau)^2.$$

An earlier investigation for an equilibrium system, for which $T(q)=T_0, \varepsilon=0$, suggested that this choice has a marked structural advantage over the Nosé-Hoover oscillator. It is ergodic, providing a complete coverage of the phase space, without stable periodic orbits. We carefully checked the ergodicity property, as explained below. In Fig. 4, we show two perspective views of a (three-dimensional) Poincaré section for the equilibrium flow. Near-equilibrium flows look much the same. With the two control variables the motion is ergodic, rather than a complex mixture of chaotic and regular regions found with a single control.

Let us illustrate the ergodicity in the equilibrium case. The equilibrium $\varepsilon=0$ Poincaré section on the left side of Fig. 4 was constructed in the usual way, by plotting a phase point whenever ζ changed sign during a Runge-Kutta time step. The view shown, along the ξ axis, shows the same disquieting gaps in the density we encountered in the previous section. The gaps reflect the linear vanishing of $\dot{\zeta}$ in the vicinity of $\{p=\pm 1\}$. Thus these gaps only indicate vanishing velocity normal to the Poincaré plane, not a lack of ergodicity. To demonstrate this, we constructed a second Poincaré section, not shown, which measured density at the Poincaré plane, as opposed to the flux across it. This second section was composed of all the points in a thin slice, of width 0.002, normal to the ζ axis. We were surprised to find that the gaps apparently persisted in this view too. But the persistence was an optical illusion, caused by the lower apparent density associated with trajectory line segments, as opposed to isolated points. Near $\{p=\pm 1\}$ most contributions to the probability density are in the form of such line segments. To show this, a run 100 times longer was analyzed, plotting every 100th point within our Poincaré slice. This third view is shown on the right side of Fig. 4, and shows no gaps at all. Finally, we computed the first four moments, $\langle |p|,p^2,|p^3|,p^4\rangle$, for all points found in the slice during this longer run, and found agreement, within about one part per thousand, with the values calculated analytically for the ergodic Gaussian distribution, $e^{-p^2/2}$.

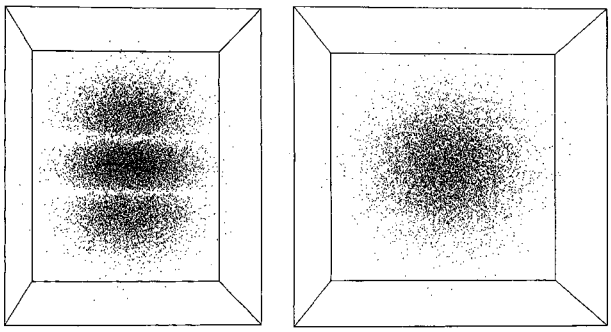

FIG. 4. Two Poincaré sections for the doubly-thermostatted oscillator of Sec. IV, with both $\langle p^2\rangle$ and $\langle p^4\rangle$ controlled. Views of $\{q,p,\xi\}$ at the hyperplane $\zeta=0$, looking down the ξ axis, are shown. Flux is shown on the left, illustrating those points crossing the plane $\zeta=0$. Density is shown at the right, rather than flux, by illustrating 1% of those points occupying a narrow slice parallel to the plane $\zeta=0$.

The difficulty in visualizing the interiors of three-dimensional Poincaré sections forced us to devise an independent convincing numerical test for ergodicity. Such a test can be based on an ensemble of Lyapunov-exponent evaluations, $\{\lambda_1\}$. The exponents are calculated for a dense set of different initial conditions, chosen on a convenient Poincaré plane. We constructed a regular grid, with 2500 initial points, $\{0<q<2,0<p<2,\zeta=0,\xi=0\}$, and computed the resulting Lyapunov exponents for trajectories composed of 100 million time steps each. If the flow equations are ergodic we would expect the long-time-averaged Lyapunov exponents all to agree. None of the various initial conditions led to a largest Lyapunov exponent very different from the mean. Further, the distribution of the 2500 values of λ_1 becomes roughly Gaussian for trajectory lengths exceeding a few tens of thousands of time steps. Then, as would be expected for an ergodic flow, the halfwidth of the distribution varies, as time increases, as the inverse square root of the number of time steps. For 100 million steps, with $dt=0.0025$, the minimum and maximum values for λ_1 in the set were 0.0654 and

TABLE III. Dependence of the Lyapunov spectrum and dissipation on the range h and strength ε of the temperature difference for a harmonic oscillator with control of the kinetic energy and its fluctuation. The results tabulated here correspond to simulations carried out for a time of 2 000 000, using a time step of 0.001. The characteristic times τ associated with the temperature control variables are equal to 0.5 and 1 as indicated. The initial condition was chosen as $(q,p,\zeta,\xi)=(0,4,0,0)$. We tabulate the full Lyapunov spectrum $\{\lambda_1,\lambda_2,\lambda_3,\lambda_4\}$ below. The sum of all exponents $\lambda_1+\lambda_2+\lambda_3+\lambda_4=-\langle\zeta+3\xi p^2\rangle$. All numbers are given in the reduced units defined in Sec. IV. The standard deviation for the nonvanishing exponents is typically ± 0.0005 for a chaotic trajectory, and less than ± 0.0001 for a limit-cycle solution. Only for $\tau=0.5$ the uncertainty of λ_4 is about twice as big. We applied Benettin's method to obtain all four time-averaged Lyapunov exponents, as is described in Refs. [21–23]. The information dimension D_I, determined according to Kaplan and Yorke, is also given.

h	ε	λ_1	λ_2	λ_3	λ_4	$\langle\zeta+3\xi p^2\rangle$	D_I
				$\tau=0.5$			
2.00	0.2	0.1571	0	−0.0159	−0.188	0.046	3.75
2.00	0.4	0.1796	0	−0.0451	−0.272	0.138	3.49
2.00	0.6	0.1708	0	−0.0626	−0.357	0.249	3.30
2.00	0.8	0.1701	0	−0.0788	−0.522	0.431	3.18
1.00	0.2	0.1677	0	−0.0247	−0.233	0.090	3.61
1.00	0.4	0.1658	0	−0.0648	−0.317	0.216	3.32
1.00	0.6	0.1626	0	−0.0710	−0.533	0.441	3.17
1.00	0.8	0.1633	0	−0.1271	−0.939	0.906	3.03
0.50	0.2	0.1595	0	−0.0218	−0.245	0.107	3.56
0.50	0.4	0.1730	0	−0.0735	−0.386	0.286	3.26
0.50	0.6	0.1740	0	−0.1086	−0.720	0.654	3.09
0.50	0.8	0.1588	0	−0.1960	−1.165	1.203	2.80
0.25	0.2	0.1576	0	−0.0223	−0.254	0.118	3.53
0.25	0.4	0.1698	0	−0.0833	−0.424	0.338	3.20
0.25	0.6	0.1653	0	−0.1346	−0.721	0.690	3.04
0.25	0.8	0.1689	0	−0.2581	−1.170	1.259	2.65
				$\tau=1.0$			
2.00	0.2	0.0673	0	−0.0010	−0.0689	0.002	3.97
2.00	0.4	0.0667	0	−0.0036	−0.0709	0.008	3.89
2.00	0.6	0.0639	0	−0.0074	−0.0773	0.021	3.73
2.00	0.8	0	−0.0018	−0.0018	−0.0456	0.049	1
1.00	0.2	0.0670	0	−0.0015	−0.0698	0.004	3.94
1.00	0.4	0.0637	0	−0.0043	−0.0751	0.016	3.79
1.00	0.6	0.0620	0	−0.0109	−0.1018	0.051	3.50
1.00	0.8	0	−0.0008	−0.0008	−0.0376	0.039	1
0.50	0.2	0.0665	0	−0.0014	−0.0704	0.005	3.93
0.50	0.4	0.0620	0	−0.0052	−0.0793	0.022	3.72
0.50	0.6	0.0638	0	−0.0130	−0.1325	0.082	3.38
0.50	0.8	0.0601	0	−0.0245	−0.1931	0.158	3.19
0.25	0.2	0.0677	0	−0.0017	−0.0738	0.008	3.90
0.25	0.4	0.0628	0	−0.0065	−0.0869	0.031	3.65
0.25	0.6	0.0641	0	−0.0215	−0.1773	0.135	3.24
0.25	0.8	0.0615	0	−0.0281	−0.2630	0.230	3.13

0.0707, respectively. We conclude, with confidence, that the nonequilibrium phase-space distribution for this four-dimensional nonequilibrium flow is, like the equilibrium one, ergodic. There can be no noticeable isolated cavities in the chaotic sea for such nonequilibrium distributions, at least sufficiently near to the equilibrium case. Thus this four-dimensional model is a relatively simple prototype for understanding many-body irreversible flows, being simultaneously time-reversible, dissipative, and ergodic. Data shown in Table III, for comparison to those found with a single control variable demonstrate the simpler nature of the four-dimensional model. However, for large temperature differences, $\varepsilon=0.8$, and a wide transition region, $h\geqslant 1$, the asymptotic solution is not chaotic but a limit cycle, if the slower of the control mechanisms involving the larger of the two investigated response times, $\tau=1.0$, is chosen. The use of two control variables, ζ and ξ, also makes the equations of motion stiffer than in the case of Sec. III. A reduced time

step of 0.001 was required for the simulations leading to Table III.

V. SUMMARY AND CONCLUSION

We have studied four distinct models for time-reversible dissipative phase-space flows. The last of them, which controls two moments of the velocity distribution, is the most promising, because the flow is ergodic near equilibrium. The many three-dimensional and four-dimensional chaotic flows explored here should prove to be useful guides to the understanding of the mathematical structure of continuous time-reversible dissipative many-body systems. Our investigations suggest that there is a qualitative difference between the relative simplicity of flows embedded in spaces of four, or more, dimensions, and the complexity of the three-dimensional flows. Thus the present work provokes an interesting mathematical question: Why is it that stable periodic orbits, and their accompanying topological complexity, are so much rarer in four dimensions than in three? Perhaps the complexity of a three-dimensional Poincaré section plays the same rôle for ergodicity as does a three-dimensional embedding space for nonlinear chaos?

Because maps are analogous to Poincaré sections, they have been studied exhaustively [18,19]. It is natural to wonder whether or not maps can be constructed which have the same characteristics as the flows studied here. Typically the attractor dimensions associated with maps are considerably less than the embedding dimension, with most maps including both singularities and periodic boundaries. The simplest time-reversible dissipative ergodic map is a two-dimensional generalized rotated Baker map, as was pointed out to us by Vance [19]. This Baker-map example, like the Galton board, and many more-complicated time-reversible dissipative maps [19], includes both singular surfaces and periodic boundaries. It is a worthy goal to seek out maps analogous to the simple dual-control system of Sec. IV.

ACKNOWLEDGMENTS

This work was performed at the University of Vienna, the University of California, the Lawrence Livermore National Laboratory, and at Warwick University. We thank all these institutions, as well as Jeroen Lamb of Warwick University, Carol Hoover of LLNL, Victor Castillo of the Department of Applied Science, University of California at Davis/Livermore, Brad Lee Holian, of the Los Alamos National Laboratory, and Aaron Vrtala of the University of Vienna for support. Carol Hoover provided useful criticism and suggestions. We gratefully acknowledge support from the Fonds zur Förderung der wissenschaftlichen Forschung, Grant No. P11428. Work performed at the Livermore Computer Center was supported by grants from the Advanced Scientific Computing Initiative and the Accelerated Strategic Computing Initiative. Work at the Livermore Laboratory was carried out under the auspices of the United States Department of Energy, pursuant to Contract No. W-7405-Eng-48.

APPENDIX

Here we extend the Hamiltonian in Nosé's original theory [15], as well as Carl Dettmann's more elegant modification of it [20], to describe an oscillator thermostatted by a space-dependent temperature, $T(q)=T_0[1+\varepsilon\tanh(q/h)]$. The two extended Hamiltonians are

$$H_{\text{Nosé}}\equiv H_{\text{Dettmann}}/s \equiv P^2/(2ms^2)+\kappa Q^2/2+\alpha P_s^2/2+kT(Q)\ln s.$$

Q and P are referred to by Nosé as ''virtual'' coordinate and momentum variables, respectively, while s and P_s represent his thermostat ''coordinate'' and its conjugate momentum, respectively. As usual, κ and k are respectively the force constant and Boltzmann's constant. The parameter α can be expressed in terms of the mean temperature T_0 and relaxation time τ of the thermostat:

$$\alpha\tau^2=1/(kT_0).$$

These two Hamiltonians both yield the same time histories for the coordinate and the friction coefficient. Nosé's original approach [13], which we do not reproduce here, is to apply ''time scaling,'' $dt_{\text{new}}=(1/s)dt_{\text{old}}$, to the equations of motion from his Hamiltonian, and then to identify ''real'' variables q and p in terms of the virtual variables as follows:

$$Q\Rightarrow q;\quad P\Rightarrow sp=ms\dot{q};\quad P_s\Rightarrow(d\ln s/dt)/\alpha=\zeta/\alpha.$$

If we eliminate p in favor of $m\dot{q}$ the resulting Nosé-Hoover oscillator equations are

$$m\ddot{q}=-\kappa q-m\zeta\dot{q}-k(dT/dq)\int_0^t\zeta(t')dt';$$

$$\dot{\zeta}=[m\dot{q}^2-kT(q)]/(kT_0\tau^2).$$

Dettmann's approach is more straightforward. His Hamiltonian leads to exactly the same motion equations provided that the numerical value of his Hamiltonian is chosen equal to zero. The equations of motion just given differ from the equations of motion given in Sec. III only in the term containing the temperature derivative, dT/dq. For the equations of motion given in this appendix, both Nosé's Hamiltonian, and Dettmann's, are constants of the motion. The more intuitive equations of motion, which we use in Sec. III, do not have this conservation property.

[1] W. G. Hoover, *Computational Statistical Mechanics* (Elsevier, Amsterdam, 1991).
[2] D. J. Evans and G. P. Morriss, *Statistical Mechanics of Nonequilibrium Liquids* (Academic, New York, 1990).
[3] G. Benettin, L. Galgani, and J.-M. Strelcyn, Phys. Rev. A **14**, 2338 (1976).
[4] S. D. Stoddard and J. Ford, Phys. Rev. A **8**, 1504 (1973).
[5] B. L. Holian, W. G. Hoover, and H. A. Posch, Phys. Rev. Lett. **59**, 10 (1987).
[6] B. Moran, W. G. Hoover, and S. Bestiale, J. Stat. Phys. **48**, 709 (1987).
[7] Ch. Dellago, H. A. Posch, and W. G. Hoover, Phys. Rev. E **53**, 1485 (1996).
[8] N. I. Chernov, G. L. Eyink, J. L. Lebowitz, and Y. G. Sinai, Phys. Rev. Lett. **70**, 2209 (1993).
[9] W. G. Hoover, H. A. Posch, B. L. Holian, M. J. Gillan, M. Mareschal, and C. Massobrio, Mol. Simul. **1**, 79 (1987).
[10] G. Gallavotti, J. Stat. Phys. **84**, 899 (1996).
[11] W. G. Hoover, E. Craig, H. A. Posch, B. L. Holian, and C. G. Hoover, Chaos **1**, 343 (1991).
[12] J. C. Sprott, Phys. Rev. E **50**, R647 (1994); W. G. Hoover, *ibid.* **51**, 759 (1995).
[13] H. A. Posch, W. G. Hoover, and F. J. Vesely, Phys. Rev. A **33**, 4253 (1986); B. L. Holian and W. G. Hoover, *ibid.* **34**, 4229 (1986).
[14] *Proceedings of the University of Warwick Conference on Time Reversibility* (December, 1996), edited by J. Lamb [Physica D (to be published)].
[15] S. Nosé, Phys. Rev. E **47**, 164 (1993); W. G. Hoover, Phys. Rev. A **31**, 1695 (1985).
[16] L. B. Lucy, Astron. J. **82**, 1013 (1977).
[17] W. G. Hoover and B. L. Holian, Phys. Lett. A **211**, 253 (1996).
[18] J. A. G. Roberts and G. R. W. Quispel, Phys. Rep. **216**, 63 (1992).
[19] W. G. Hoover, O. Kum, and H. A. Posch, Phys. Rev. E **53**, 2123 (1996).
[20] C. Dettmann (private communication); C. P. Dettmann and G. P. Morriss, Phys. Rev. E **55**, 3693 (1997).
[21] G. Benettin, L. Galgani, A. Giorgilli, and J.-M. Strelcyn, Meccanica **15**, 9 (1980).
[22] A. Wolf, J. B. Swift, H. L. Swinney, and J. A. Vastano, Physica D **16**, 285 (1985).
[23] H. A. Posch, W. G. Hoover, and B. L. Holian, Ber. Bunsenges. Phys. Chem. **94**, 250 (1990).